D3.5 – Evaluation of pressed IC and coatings

PROJECT INFORMATION

GRANT AGREEMENT NUMBER	826323
PROJECT FULL TITLE	Low Cost Interconnects with highly improved Contact Strength for SOC Applications
PROJECT ACRONYM	LOWCOST-IC
FUNDING SCHEME	FCH-JU2
START DATE OF THE PROJECT	1/1-2019
DURATION	36 months
CALL IDENTIFIER	H2020-JTI-FCH-2018-1
PROJECT WEBSITE	www.lowcost-ic.eu

DELIVERABLE INFORMATION

WP NO.	3
WP LEADER	Forschungszentrum Jülich
CONTRIBUTING PARTNERS	Chalmers University of Technology, Borit, Sunfire
NATURE	
AUTHORS	Mareddy Reddy, Jan Froitzheim
CONTRIBUTORS	
CONTRACTUAL DEADLINE	
DELIVERY DATE TO EC	

DISSEMINATION LEVEL

PU	Public	X
PP	Restricted to other programme participants (incl. Commission Services)	
RE	Restricted to a group specified by the consortium (incl. Commission Services)	
CO	Confidential, only for the members of the consortium (incl. Commission Services)	

1 Introduction

Ferritic steels are a popular choice of interconnect materials for planar fuel cells operating between 600°C to 900°C owing to their strength, stability, ease of manufacturing, and cost. Chromia forming ferritic steels are particularly suitable for interconnects as they have better electric conductivity than alumina forming ferritic steels in the operating temperatures of a SOFC. However, oxidation and corrosion of steel interconnects is a significant concern for the lifetime and efficiency of a fuel cell. Also, chromia reacts with water vapor in the air leading to the formation of Cr^{+6} species, such as $CrO_2(OH)_2$. These volatile Cr^{+6} species react with the cathode, transforming into Cr^{+3}, which is deposited on the triple-phase boundaries. These deposits, thus block the electrochemical oxygen reaction process, leading to faster stack degradation and decreased efficiency.

Applying coatings to minimize chromium evaporation and oxidation on interconnect steels has become a widespread technique in recent times. Of all the coatings, $(CoMn)_3O_4$ spinel shows very promising results for the prevention of chromium evaporation and reduction of the corrosion rate. The coating can be deposited using various methods such as dip coating, electrophoretic deposition (EPD), screen printing, aerosol spray deposition, atmospheric plasma spray coatings, and physical vapor deposition[1–5]. Irrespective of the deposition process, the coatings are usually applied in a batch process, which is rather an inefficient process for mass production. The coatings use $(Mn,Co)_3O_4$ powder as raw material, which is relatively expensive. Finally, the coatings are processed through costly sintering steps in reducing and oxidizing environments to achieve sufficient coating density.

The process of pre-coating and subsequent shaping reduces logistics and handling costs while streamlining the process and enabling mass production of the interconnects. Physical vapor deposition (PVD) is used to apply metallic coatings on the steel by a roll-to-roll process, which facilitates high efficiency and allows for high volume production. Due to the subsequent shaping step, oxides are not suitable for this process because of their brittleness; in contrast, metallic coatings possess a much higher ductility.

When a pre-coated steel is shaped into the interconnect, it may lead to cracks and delamination of the coating. The cracks tend to appear in the areas which undergo significant deformation during the shaping process. These cracks and delaminated areas will lead to an increase in chromium evaporation, which in turn leads to the degradation of the fuel cell, reducing stack lifetime. The main prerequisites for the coating to be used in precoating and subsequent shaping of steel interconnects are

1. To be able to heal the cracks and delaminated areas on the coating.
2. Efficiently decrease the oxidation and chromium evaporation at a very low thickness

The objective of this study is to investigate the impact of shaping the coated steel into interconnects on coating performance. This impact is quantified using the chromium evaporation in the interconnect steels.

2 Materials and Methods:

Ferritic stainless steel, K44M with a thickness of 0.5mm, supplied by Aperam, was used in this work. The composition can be found in table 1. The steel was precoated with state-of-the-art cerium cobalt coating with a 10 nm cerium layer beneath a 640 nm thick cobalt layer. The coatings were applied by Sandvik Materials Technology (SMT) using a proprietary Physical Vapor Deposition (PVD) technique in a high-volume roll-to-roll process. The coated steel sheet was shaped into samples that represent certain features of the interconnect design of Sunfire. Hydroforming technology was used by Borit to shape the samples. Figure 1 shows the shaped steel sheet in the as-received condition. The shaped sheets were further cut into small coupons (figure 1) of 15 x 15 mm to be placed inside the reactor. Before the exposure, the coupons were ultrasonically cleaned in acetone and ethanol for 20 minutes each in an ultrasonic bath.

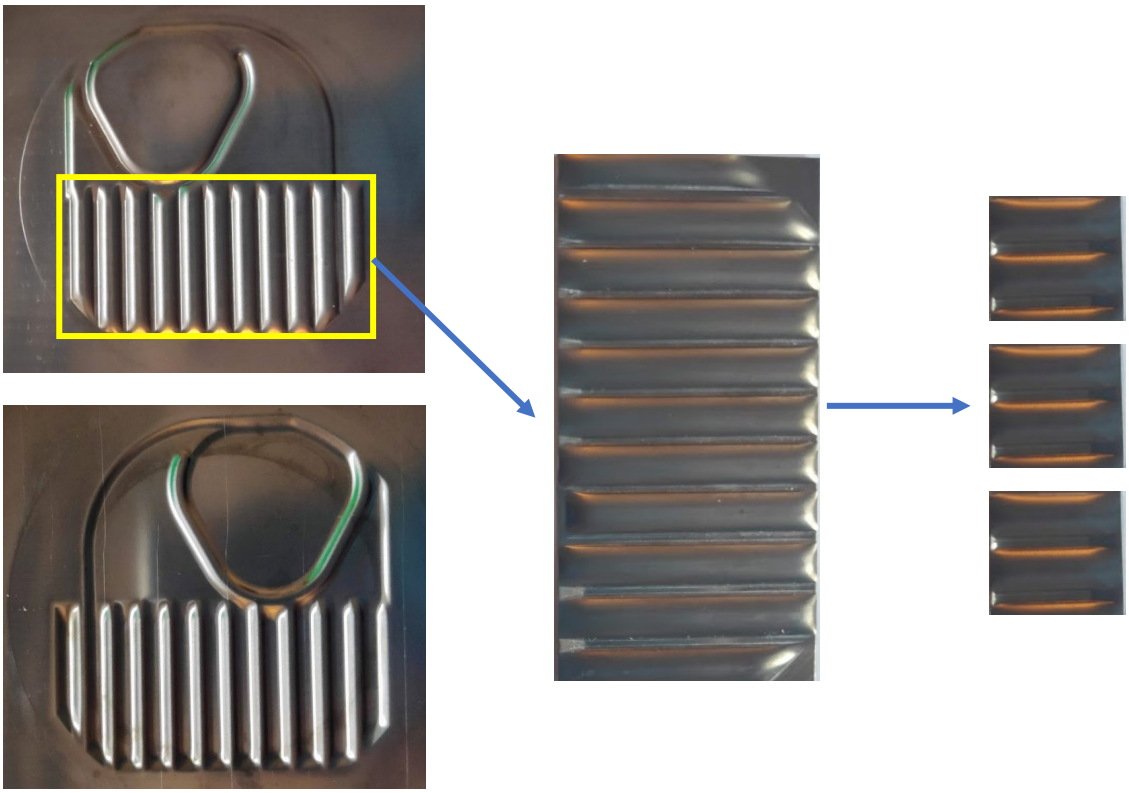

Figure 1: Shaped sheets supplied by Borit which are subsequently cut into small coupons

To simulate similar conditions experienced by Sunfire's interconnect, all the samples were isothermally exposed to 850 °C in a horizontal quartz tube reactor for 310 hours. The atmosphere around the samples was air humidified with 3% H_2O. To obtain 3% H_2O, dry air was bubbled through a water bath at elevated temperature, which was connected to a condenser maintained at a temperature of 24.4 °C. An airflow of 6000 sml min^{-1} was selected, which corresponds to an average gas velocity of 27 cm/s to ensure a flow independent regime inside the reactor. Additionally, a porous SiC flow restrictor was placed in front of the samples to obtain a uniform flow and minimize the natural convection. The samples (three coupons per exposure) were placed parallel to the direction of airflow. Figure 2 shows the experimental setup.

The chromium evaporation setup consists of a silica tube (denuder) coated with Na_2CO_3. The downstream of the samples the air from the reactor was passed through the coated denuder to capture the Cr^{+6} species. The chromium species $CrO_2(OH)_2$ react with Na_2CO_3 according to the following reaction:

$$Cr_2O_2(OH)_2(g) + Na_2CO_3(s) \rightarrow Na_2CrO_4(s) + H_2O(g) + CO_2(g)$$

The denuder was replaced at regular intervals without affecting the samples. The denuder was subsequently leached with distilled water. The chromium species in the solution were quantified by spectrophotometry using an Evolution 60S Thermo Scientific spectrometer. After the exposure, the samples were cooled slowly to the room temperature. Further details about the exposure setup can be found in Froitzheim et al.[6]. The surface morphology of as-received samples was analyzed using an SEM. Cross-sections of the exposed coupons were prepared using a broad ion beam (BIB). The microstructural and chemical composition of the oxide layer was investigated with the help of JEOL JSM-7800F Prime SEM equipped with an Oxford Instruments Energy Dispersive X-ray spectrometer (EDS).

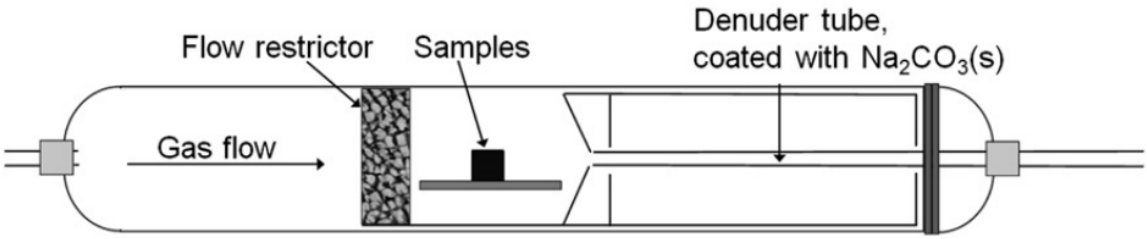

Figure 2: Schematic drawing of the reaction chamber used for the exposures

Table 1: Composition of K44M in weight%

Composition	C	Si	Mn	P	S	Cr	Ti	Nb	N	Mo	Fe
K44M	0,013	0,037	0,3	0,021	0,0005	18,92	0,003	0,56	0,015	1,85	Bal

3 Results:

3.1 Chromium evaporation:

Figure 3 shows the data from time-resolved chromium evaporation of the samples exposed to 850 °C for 310 hours. It shows the rate of Cr evaporation as a function of exposure time for the shaped steel sheet. The horizontal band shows the spread of Cr evaporation rate on the undeformed Co/Ce coated K44M steel exposed to the same conditions. . The evaporation rate of K44M at 850 °C is similar to that of other ferritic steels such as AISI 441 or Crofer 22 APU. The rate of Cr evaporation is higher for the shaped samples during the first 50 hours into the exposure. However, the chromium

evaporation reduced with an increase in the exposure time to levels of undeformed Co/Ce coated material. The decrease in the chromium evaporation indicates that the coating is healing with time.

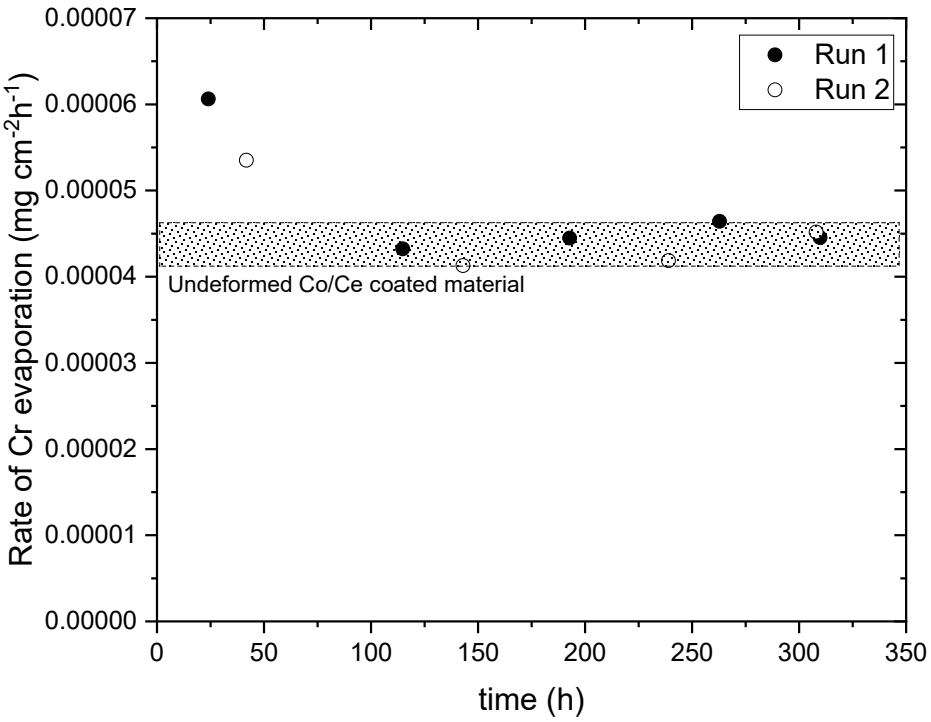

Figure 3: Chromium evaporation rate of shaped interconnect exposed for 310 hours in air with 3% H2O with a flow rate of 6000 sml min^{-1}

3.2 Microstructure:

3.2.1 Pre-exposure coupons:

Figures 4a, c shows the location on the as-received specimen off the 'hill' and 'valley', respectively. Figures 4b, d are SEM micrographs showing the surface morphology at the respective locations. The pre-coated steel shaped into the interconnects (as received sample) showed severe crack formation in the coating. The coating cracks are more prevalent in the regions that experienced the maximum amount of tensile deformation. The 'hill' (figure 4b) shows significant cracking and delamination of the coating owing to much higher tensile deformation than the 'valleys' (figure 4d), which showed little cracking and no delamination. Similar cracking and delamination of the Ce/Co coating upon shaping on 0.2mm thick Sanergy HT is reported in the literature [7].

3.2.2 Post-exposure coupons:

Figures 5 & 6 show the cross-section micrographs on the 'hill' and the 'valley' of the samples exposed to 850°C for 310 hours, respectively. The cross-section micrographs on the hill (figure 5),

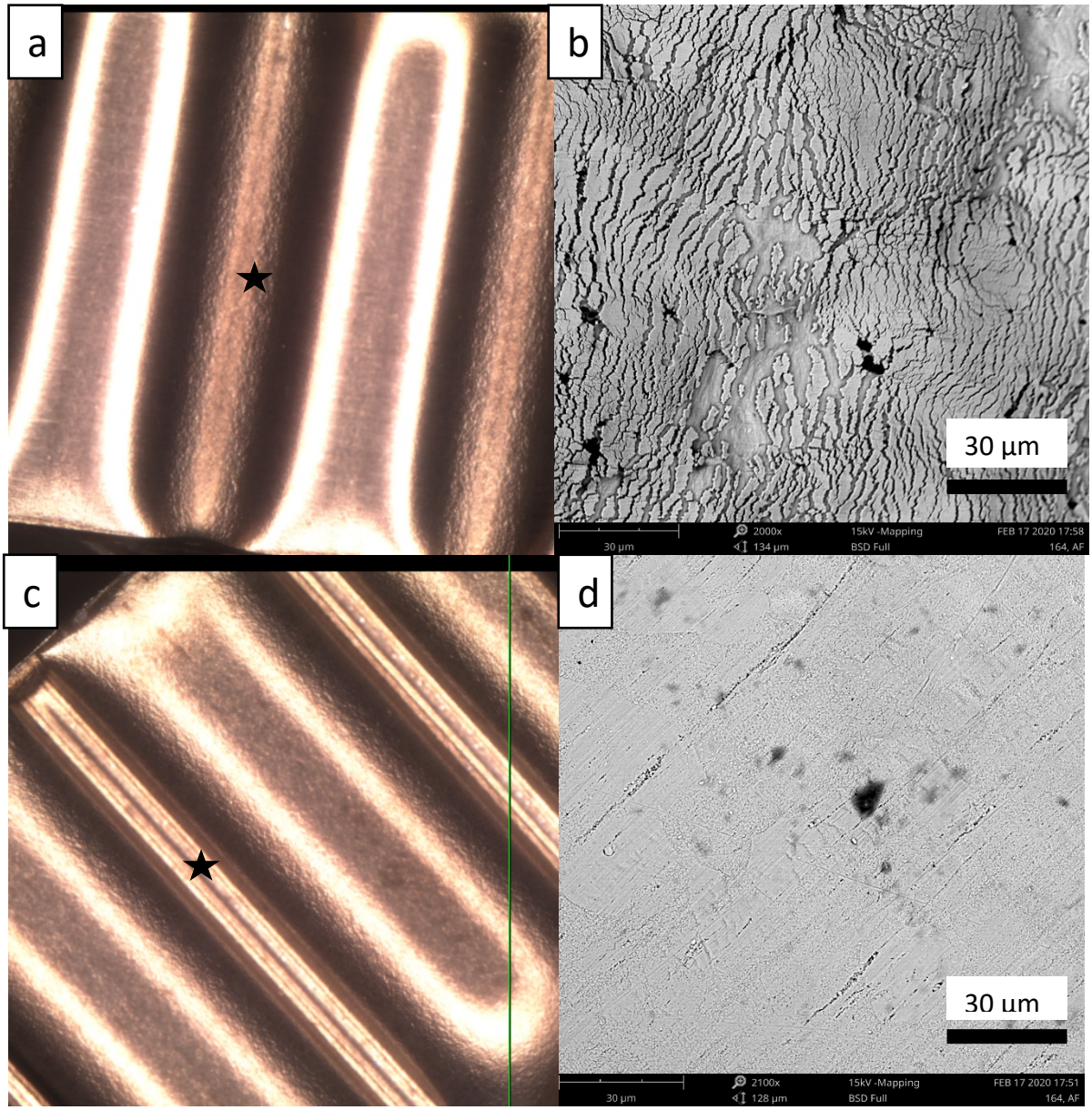

Figure 4: Images a, c shows the optical micrographs of the as-received interconnects pointing 'hill' and 'valley' respectively. Images b, d are SEM micrographs showing the surface morphology of the coating at the location specified in the images a, c, respectively.

which experienced the most severe cracks in the coating (Figure 4b), show a uniform two-layered oxide on the surface. Figure 7 shows the EDX elemental maps of the elements Cr, Co, and Mn in the cross-section of the 'hill' at two locations specified. The elemental map of Co is dense and uniform throughout the oxide scale. Beneath the Co layer lies the chromia layer, which is continuous throughout the scale. Moreover, the enrichment of Mn on the surface indicates the formation of $(Co,Mn)_3O_4$ spinel. The formation of the Co-Mn spinel on the top of the chromia layer decreases the rate of chromium evaporation. The chromium evaporation data (figure 3) indicates that it took about 50 hours for the rate of chromium evaporation to decrease to similar levels as in undeformed samples.

The cross-section micrographs on the valley area (figure 6) showed only minimal cracks (figure 4d) in the coating and show a uniform two-layered oxide on the surface. Figure 8 shows the EDX elemental maps in the cross-section of the valley. The maps show that the outer oxide is rich Co and Mn ($(Co,Mn)_3O_4$), and the layer beneath is a chromia ((Cr_2O_3)) layer beneath it similar to the oxide scale on the hill.

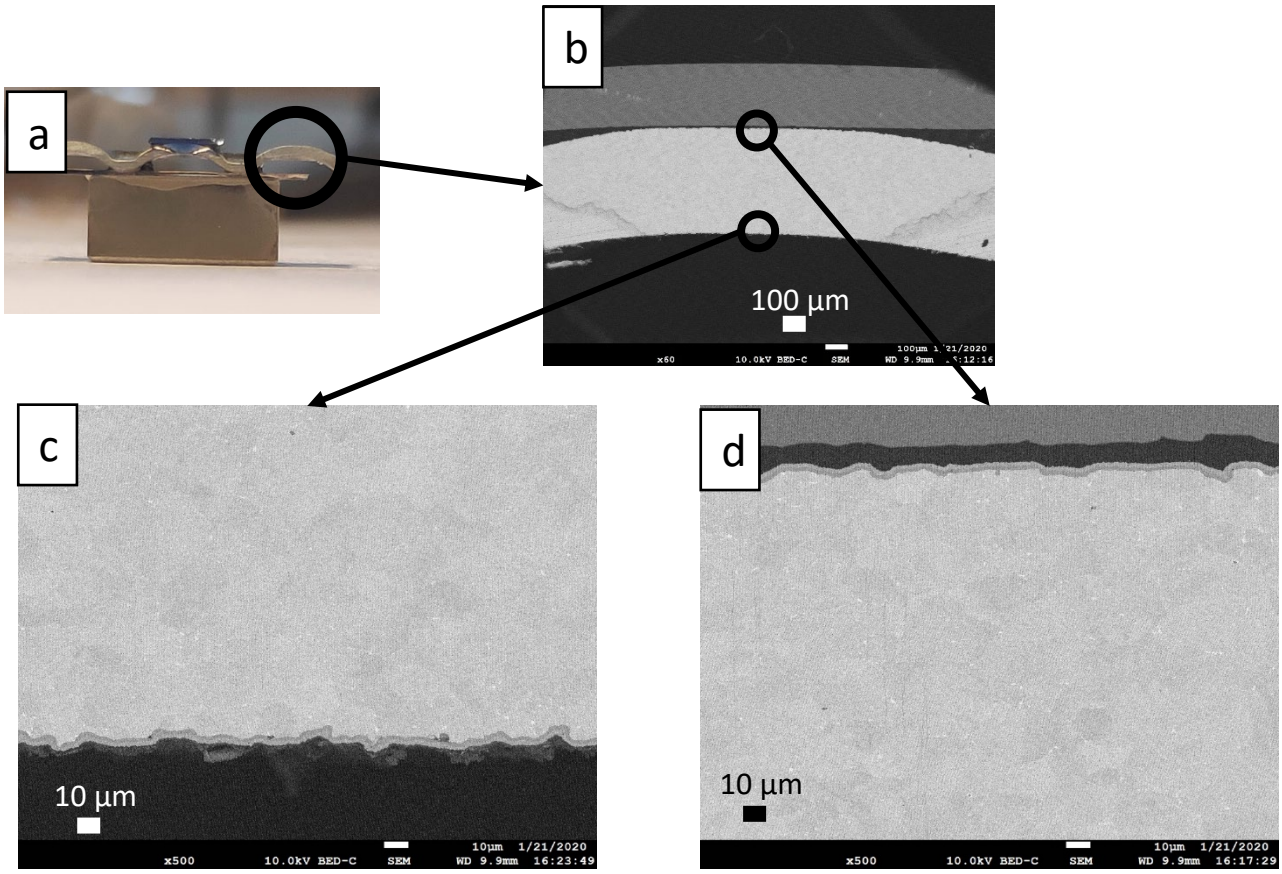

Figure 5: (a) Location of the 'hill' on the stamped interconnect, (b) BIB cross-section micrograph of the milled cross-section on the hill. Images c, d shows the BIB cross-section micrographs of the milled cross-sections at the locations shown in the image b.

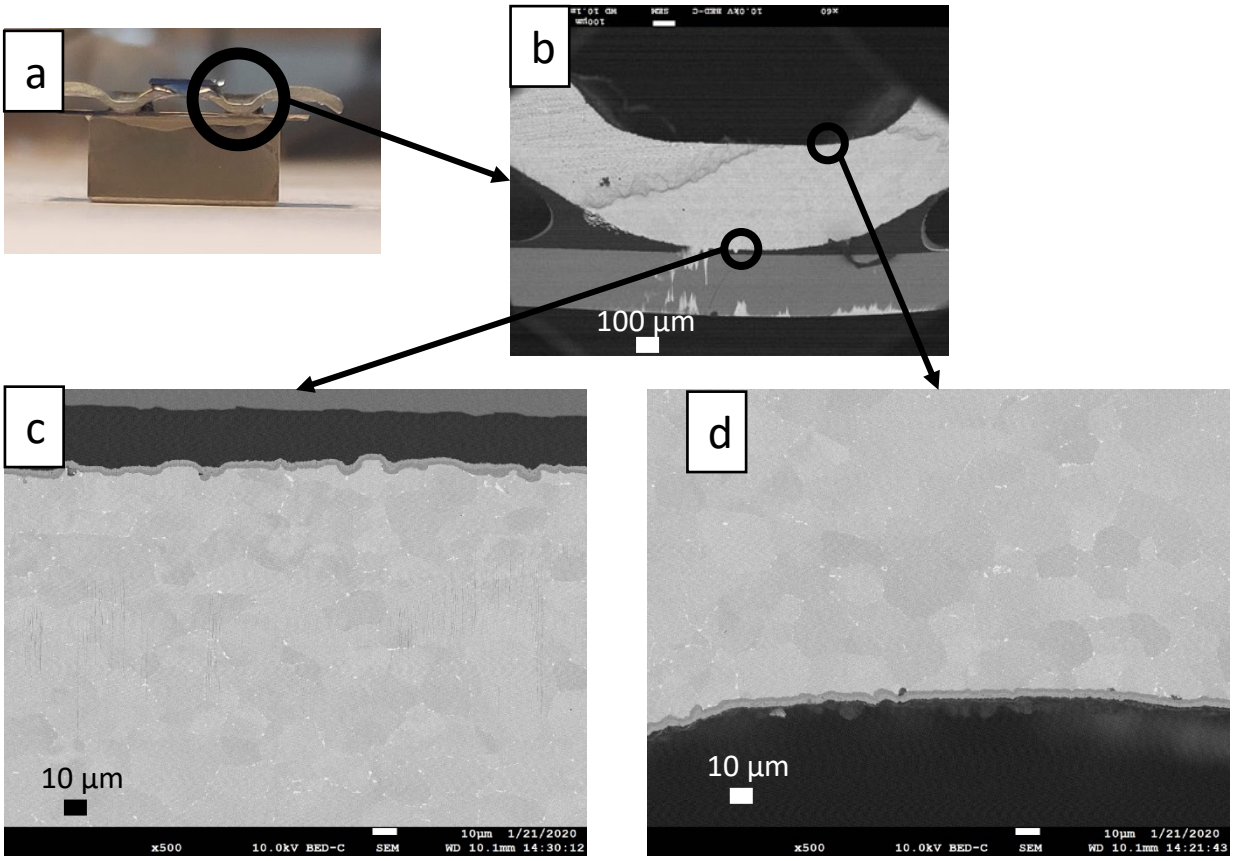

Figure 6: (a) Location of the 'valley' on the stamped interconnect, (b) BIB cross-section micrograph of the milled cross-section. Images c, d shows the BIB cross-section micrographs of the milled cross-sections at the locations shown in the image b.

The Oxidation of the metallic cobalt layer leads to volumetric expansion of the coating as the Co converts to Co_3O_4. Thus, minor cracks in the coating may heal due to this volumetric expansion associated with the oxidation of the coating. In Mn containing steels, the Mn in steel diffuses to the surface to form spinel oxides [7–9]. Hence, $(Co,Mn)_3O_4$ spinel is seen on the top of the oxide scale after 310 hours of exposure. Similarly, in the absence of the coatings, $(Cr,Mn)_3O_4$ spinel is seen on the top of the oxide layer only within 24 hours[7, 8]. In the regions with cracked coating, $(Cr,Mn)_3O_4$ spinel is formed due to the absence of the cobalt. $(Co,Mn)_3O_4$ spinel is formed on the top of the oxide layer in the areas with intact coating.

Due to the presence of Co, the oxide layer in the regions with an intact coating is thicker than the cracked areas. Nevertheless, during continued exposure to high temperature, fast surface diffusion occurs between the spinel oxides $(Co,Mn)_3O_4$, and $(Cr,Mn)_3O_4$ to form $(Co,Mn)_3O_4$ with traces of Cr. Hence a homogenous distribution of Co, Mn, Cr is seen in the oxide layer with continued exposure. Due to the formation of continuous $(Co,Mn)_3O_4$ on the surface, the chromium evaporation is the same as for the undeformed material.

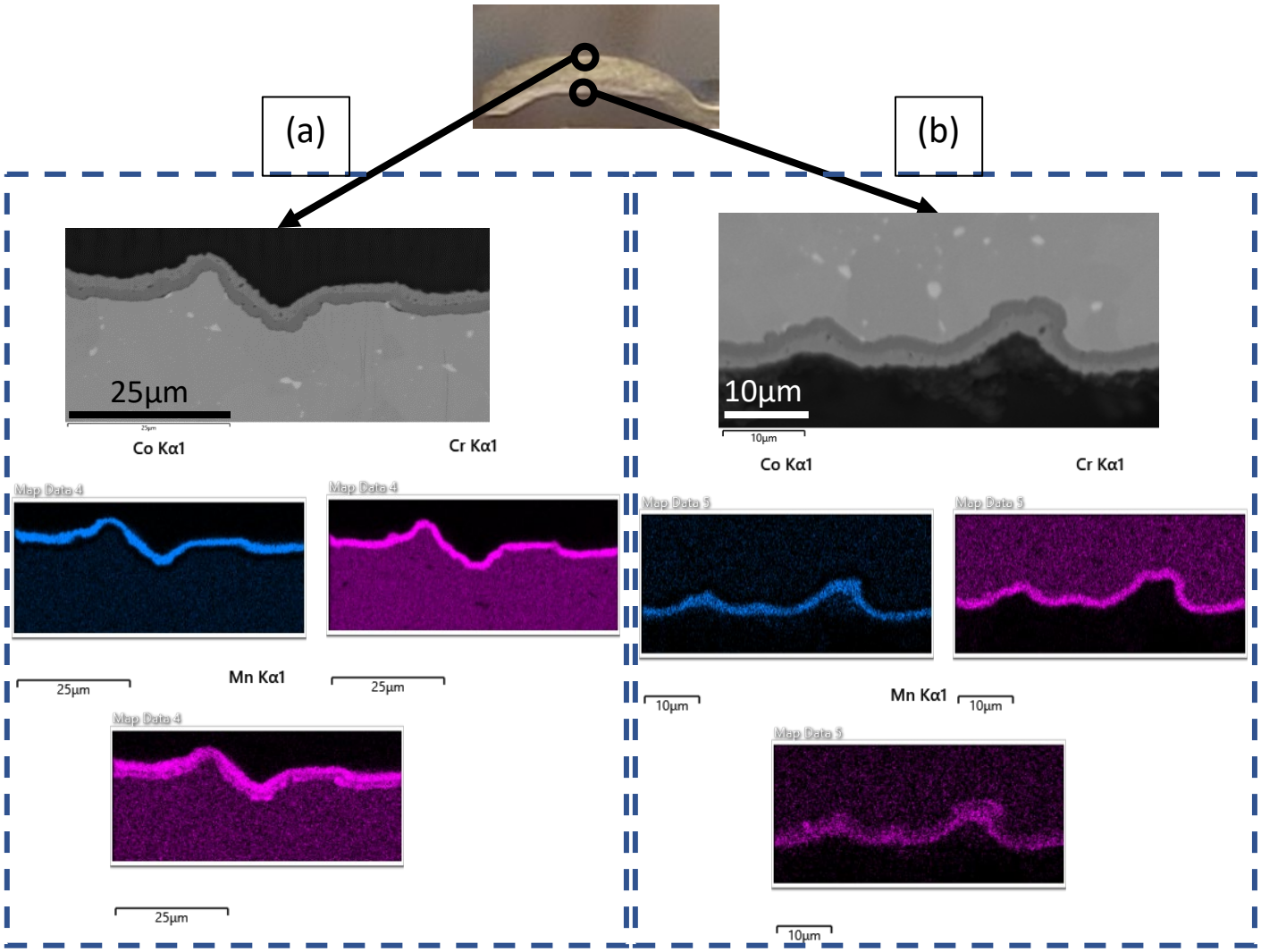

Figure 7: BIB cross-section SEM image and EDX elemental maps in the 'hill' of shaped interconnect coupon exposed for 310 hours in air with 3% H_2O with a flow rate of 6000 sml min^{-1}

3.3 Effect of temperature

Since the observed self-healing effect depends on diffusion it is not obvious whether to the found results also hold true for lower temperatures. In order to investigate this a set of Co/Ce coated samples was tested at 650 and 750 °C. 650 °C is commonly seen as the lower end of operating temperatures for SOFC and probably represents a worst-case scenario. Due to experimental constraints these experiments were performed on AISI 441 material that was bi-axially deformed (15 %). Cr evaporation measurements revealed that the Cr evaporation rate is indeed higher in the initial phase of exposure, although still much lower than uncoated material. Nevertheless, the Cr evaporation rate drops quickly and approaches levels very similar to the ones of undeformed material within less than 100h at 750 oC and less than 200h 650 °C.

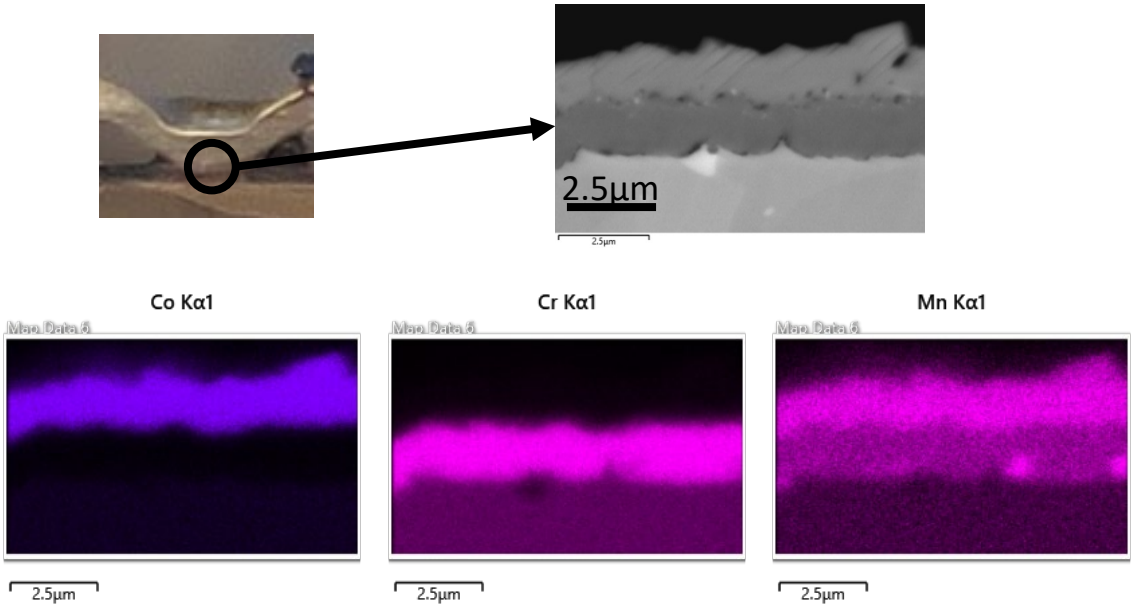

Figure 8: BIB cross-section SEM image and EDX elemental maps in the 'valley' of shaped coupon exposed for 310 hours in air with 3% H_2O with a flow rate of 6000 sml min^{-1}

4 Conclusions:

In this study, the impact of shaping (mechanical deformation) the pre-coated steels into interconnects is studied with the help of chromium evaporation measurements and microscopy. Mechanical deformation of the pre-coated steels showed crack formation in some regions of the interconnect. The rate of chromium evaporation is higher in the first 24 hours due to the cracks in the coating. However, only after 50 hours at 850 °C, the rate of chromium evaporation decreased to similar levels as in undeformed Ce/Co coated steel. Similarly, the chromium evaporation quickly dropped to the levels of undeformed Ce/Co coated steel at 750 °C and 650 °C after 100 hours and 200 hours, respectively. Cross-sectional microstructure and chemical analysis showed a continuous cobalt rich layer on the entire surface. During the exposure of the shaped steels, the smaller cracks healed due to the volume expansion of the coating upon oxidation. The regions with larger cracks and delaminated areas formed $(Cr,Mn)_3O_4$ initially. However, the interdiffusion of the spinels $(Co,Mn)_3O_4$, $(Cr,Mn)_3O_4$ on the surface led to the formation of a uniform $(Co,Cr,Mn)_3O_4$. This, in turn, led to homogenous distribution of Co, Mn, Cr is seen in the oxide layer with $(Co,Mn)_3O_4$ as a cap on the chromia scale, protecting from chromium evaporation.

5 References:

1. Talic B, Molin S, Hendriksen PV, Lein HL. Effect of pre-oxidation on the oxidation resistance of Crofer 22 APU. *Corros Sci*. 2018;138:189–199. https://doi.org/10.1016/j.corsci.2018.04.016
2. Falk-Windisch H, Svensson JE, Froitzheim J. The effect of temperature on chromium vaporization and oxide scale growth on interconnect steels for Solid Oxide Fuel Cells. *J Power Sources*. 2015;287:25–35. https://doi.org/10.1016/j.jpowsour.2015.04.040
3. Spotorno R, Piccardo P, Perrozzi F, Valente S, Viviani M, Ansar A. Microstructural and Electrical Characterization of Plasma Sprayed Cu-Mn Oxide Spinels as Coating on Metallic Interconnects for Stacking Solid Oxide Fuel Cells. *Fuel Cells*. 2015;15(5):728–734. https://doi.org/10.1002/fuce.201400189
4. Talic B, Wulff AC, Molin S, Andersen KB, Zielke P, Frandsen HL. Investigation of electrophoretic deposition as a method for coating complex shaped steel parts in solid oxide cell stacks. *Surf Coatings Technol*. 2019;380. https://doi.org/10.1016/j.surfcoat.2019.125093
5. Grünwald N, Sohn YJ, Yin X, Menzler NH, Guillon O, Vaßen R. Microstructure and phase evolution of atmospheric plasma sprayed Mn-Co-Fe oxide protection layers for solid oxide fuel cells. *J Eur Ceram Soc*. 2019;39(2–3):449–460. https://doi.org/10.1016/j.jeurceramsoc.2018.08.027
6. Froitzheim J, Larsson E, Johansson L-G, Svensson J-E. Cr Evaporation of Metallic Interconnects: A Novel Method for Quantification. The Electrochemical Society; 2009:1423–1428. https://doi.org/10.1149/1.3205674
7. Falk-Windisch H, Sattari M, Svensson JE, Froitzheim J. Chromium vaporization from mechanically deformed pre-coated interconnects in Solid Oxide Fuel Cells. *J Power Sources*. 2015;297:217–223. https://doi.org/10.1016/j.jpowsour.2015.07.085
8. Sachitanand R, Sattari M, Svensson JE, Froitzheim J. Evaluation of the oxidation and Cr evaporation properties of selected FeCr alloys used as SOFC interconnects. *Int J Hydrogen Energy*. 2013;38(35):15328–15334. https://doi.org/10.1016/j.ijhydene.2013.09.044
9. Goebel C, Berger R, Bernuy-Lopez C, Westlinder J, Svensson JE, Froitzheim J. Long-term (4 year) degradation behavior of coated stainless steel 441 used for solid oxide fuel cell interconnect applications. *J Power Sources*. 2020;449. https://doi.org/10.1016/j.jpowsour.2019.227480

Acknowledgment

This project has received funding from the Fuel Cells and Hydrogen 2 Joint Undertaking under grant agreement No 826323. This Joint Undertaking receives support from the European Union's Horizon 2020 research and innovation programme, Hydrogen Europe and Hydrogen Europe research.